Science of the Total Environment 1046 (2026) 182017

Contents lists available at ScienceDirect

Science of the Total Environment

journal homepage: www.elsevier.com/locate/scitotenv

# Environmental variables improve remote sensing-based water table monitoring in peatlands

Priscillia Christiani [a,b,*], Aleksi Räsänen [b], Anton Kuzmin [c], Paavo Ojanen [d,e], Kari Minkkinen [e], Pasi Korpelainen [c], Parvez Rana [d], Timo Kumpula [c], Aleksi Isoaho [a]

[a] Natural Resources Institute Finland (Luke), Paavo Havaksen tie 3, FI-90570, Oulu, Finland
[b] Geography Research Unit, University of Oulu, P.O. Box 8000, FI-90014, Finland
[c] Department of Geographical and Historical Studies, Faculty of Social Sciences and Business Studies, University of Eastern Finland, P.O. Box 111, FI-80101, Joensuu, Finland
[d] Natural Resources Institute Finland (Luke), Latokartanonkaari 9, Helsinki, FI-00790, Finland
[e] Department of Forest Sciences, University of Helsinki, P.O. Box 27, FI-00014, Finland

## HIGHLIGHTS

- Optical remote sensing alone has limitations in monitoring peatland water table (WT).
- We assess whether the inclusion of environmental variables improves WT models.
- Topographic variables improve spatial WT models in northern aapa mires.
- Canopy height model and depth to water improve spatiotemporal WT models in a drained peatland forest.

## GRAPHICAL ABSTRACT

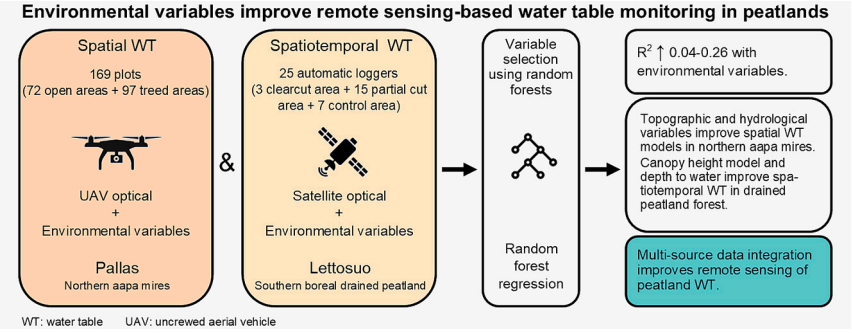


## ARTICLE INFO

*Keywords:*
Mire
Drone
UAV
Satellite
Moisture
Hydrology
Fen
Peatland

## ABSTRACT

Water table (WT) is a key indicator of peatland ecosystem functioning, but its spatiotemporal monitoring is challenging. Optical remote sensing has been used in peatland WT monitoring with varying success, but few studies have tested whether environmental variables—particularly topographic and tree stand structure variables derived from LiDAR—improve modelling performance. We tested whether environmental variables improve (1) uncrewed aerial vehicle-derived spatial WT models in two northern boreal, partly drained aapa mires and (2) satellite image-derived spatiotemporal WT models in a southern boreal drained peatland forest in Finland. We employed random forest regression and variable selection techniques to model WT, using optical remote sensing and environmental variables as predictors. Our results showed that environmental variables related to topography and tree stand structure improve modelling performance, with $R^2$ increasing by 0.01–0.19 compared to optical-only models. Our findings support the integration of optical and environmental data for spatial and spatiotemporal WT monitoring in boreal peatlands.

* Corresponding author at: Natural Resources Institute Finland (Luke), Paavo Havaksen tie 3, FI-90570, Oulu, Finland.
*E-mail address:* priscillia.christiani@luke.fi (P. Christiani).

https://doi.org/10.1016/j.scitotenv.2026.182017
Received 30 September 2025; Received in revised form 22 June 2026; Accepted 30 June 2026
Available online 2 July 2026

## 1. Introduction

Peatlands store nearly 30% of terrestrial carbon despite covering only 3% of the global land surface (Minasny et al., 2023; J. Xu et al., 2018). They also sustain unique biota and provide essential ecosystem services, such as catchment water management, biodiversity conservation, and recreational areas (Ramchunder et al., 2012; Juutinen et al., 2024). The water table (WT) is an important indicator for peatland condition, as it is closely connected to ecosystem properties such as peat subsidence, greenhouse gas dynamics, and vegetation patterns (Evans et al., 2021; Ma et al., 2022; Koch et al., 2023; Albert-Saiz et al., 2025). WT is closely linked to peatland wetness, especially in *Sphagnum*-dominated peatlands, in which capillary connectivity keeps the surface saturated (Rydin et al., 2006; Thompson and Waddington, 2008). In fens and *Carex*-dominated peatlands, the relationship is weaker due to higher hydraulic conductivity and greater microtopographic variability (Ahmad et al., 2025; Crockett et al., 2016). WT is commonly monitored due to its straightforward measurement protocol (e.g., dipwells) and its comparability across different sites (Albert-Saiz et al., 2025). However, point-based measurements capture only localized conditions and may not provide a good overall representation of WT across an entire peatland complex. Furthermore, spatially and temporally comprehensive monitoring is challenging because peatlands are often large in extent and located in remote regions.

Remote sensing is widely used to monitor WT dynamics. While WT cannot be directly measured using remote sensing, remotely sensed data can serve as proxies for various factors linked to WT, including land cover, surface moisture, vegetation greenness and structure, and microtopography. In particular, optical and radar satellite- and uncrewed aerial vehicle (UAV)-based observations are commonly used for temporal WT analyses (Bechtold et al., 2018; Asmuß et al., 2019; Räsänen et al., 2022; Burdun et al., 2023; Isoaho et al., 2023). Beyond optical and radar sensors, airborne geophysical techniques—such as electromagnetic induction and ground-penetrating radar—can provide additional information on peat properties and moisture (Henrion et al., 2024; Trappe and Kneisel, 2019). Nevertheless, relatively few studies have focused on upscaling plot-level WT measurements into spatially continuous maps across heterogeneous peatland environments (e.g., Kalacska et al., 2018; Isoaho et al., 2023, 2024).

Of the different remote sensing techniques, optical remote sensing has generally performed best in modelling WT in boreal peatlands (Räsänen et al., 2022; Burdun et al., 2023; Isoaho et al., 2024), largely because surface reflectance and vegetation indices act as indirect indicators of peat surface moisture conditions and WT (Jackson et al., 2004; Sadeghi et al., 2017). Optical data have performed better in open peatlands, where the optical signal originates mainly from ground vegetation (Räsänen et al., 2022; Burdun et al., 2023) than in forested peatlands, where dense tree canopies obscure the ground surface signal, reducing the sensitivity of optical data to detect near-surface wetness. This canopy effect is an important limitation, especially because many peatlands—both naturally and due to historical drainage—have substantial tree cover (e.g., Ikkala et al., 2022). Radar data, particularly at commonly used C-band frequencies, also face limitations because penetration depths are shallow and backscatter is strongly influenced by canopy structure (Bechtold et al., 2018; Millard and Richardson, 2018). Consequently, optical data often outperform radar, although multisensor approaches combining both have yielded the best overall WT modelling results (Räsänen et al., 2022; Isoaho et al., 2024; Reddin et al., 2025).

Environmental variables have the potential to improve remote sensing-based ecosystem mapping in peatlands (Ghazaryan et al., 2024). Earlier studies have shown that vegetation patterns and greenhouse gas fluxes in peatlands can be better modelled through the combined use of optical and environmental data (Räsänen et al., 2020; Koch et al., 2023). In particular, digital elevation model (DEM) and their derivatives have been important predictors in modelling vegetation patterns (Harris and Baird, 2019; Liang and Wang, 2020). Still, only a few studies have tested the relationship between topography and peatland wetness (Ikkala et al., 2022; Isoaho et al., 2023; Reddin et al., 2025). Additionally, some empirical studies have shown that the effects of drainage on peatland WT depend on the distance to drainage ditches (Braekke, 1983; Haapalehto et al., 2014), but this relationship has not been widely studied. Despite these studies, few have utilised optical data together with environmental data for WT monitoring in peatlands.

We use spatial and spatiotemporal WT measurements from two study regions in Finland to investigate whether environmental variables can enhance optical remote-sensing-based WT modelling. Specifically, our objectives are to assess whether LiDAR-derived environmental variables improve (1) models depicting spatial patterns of WT based on ultra-high-resolution UAV data in heterogeneous aapa mire complexes, and (2) models capturing spatiotemporal WT patterns based on medium- to high-spatial-resolution satellite imagery in drained peatland forests.

## 2. Materials and methods

### 2.1. Study sites and field data

We studied three sites located in two regions of Finland (Fig. 1). In northern Finland, Matorovansuo and Välisuo (hereafter collectively referred to as Pallas) are aapa mires; i.e., concave mires in which central areas are minerotrophic and include wet flarks (Eurola et al., 1995; Laitinen et al., 2007). Both sites have undergone drainage along the peatland edges in the 1960s but have remained relatively wet and treeless in the undrained areas. The open areas contain typical northern aapa mire vegetation, such as various graminoids (e.g., *Carex magellanica*, *Eriophorum vaginatum,* and *Trichophorum cespitosum*) and *Sphagnum* mosses (e.g., *S. lindbergii*, *S. jensenii* and *S. fuscum*). The wettest open areas are flark fens characterized by flark–string patterns i.e., water-filled depressions (flarks) alternating with drier hummocks (strings). In the drained and treed areas, there is abundant tree cover dominated by Scots pine (*Pinus sylvestris*) and Norway spruce (*Picea abies*), which have become denser after drainage. Forest vegetation (e.g., *Pleurozium schreberi* and *Vaccinium myrtillus*) has partly replaced typical peatland vegetation in the ground and field layers. For our analyses, we divided the Pallas region into open and treed areas (Fig. 1).

Lettosuo is located in southern Finland and is a nutrient-rich drained peatland forest. The site was first partially drained in the 1930s and more extensively in the 1960s. In 2016, the site was experimentally harvested for impact monitoring using three different treatments: (1) a clearcut area where all trees were removed, (2) a partial cut area in which all dominant pines were harvested, and (3) a control area that remained untouched during the harvesting (Korkiakoski et al., 2023). The current tree stand consists of Norway spruce, downy birch (*Betula pubescens*), and Scots pine, with substantial variation in tree size and species distribution across the different treatments.

We defined WT relative to the local peatland surface with centimetre-level accuracy (WT $< 0$ below the surface; WT $> 0$ above the surface). In Pallas, we manually measured WT using perforated plastic standpipe wells installed in the peat soil (see Heikkinen et al., 2026). In total, we measured WT at 169 measurement points (72 in treed areas and 97 in open areas) between 23 and 25 July 2023 (Table 1; Fig. 1). In Lettosuo, 25 automatic loggers (Odyssey® Capacitance Water Level Logger, Dataflow Systems Ltd., New Zealand) were installed in perforated plastic standpipe wells to monitor WT during the growing seasons of 2017–2023. Of these loggers, three were placed in the clearcut area, 15 in the partial-cut area, and seven in the control area (Table 1; Fig. 1). The loggers recorded data hourly, and we calculated daily averages for modelling purposes.

### 2.2. Collecting and processing drone data

We used a DJI Matrice 300 RTK UAV to collect multispectral imagery

(MicaSense Altum-PT) and LiDAR data (YellowScan mapper+) for Pallas on 22–24 July 2023. Flights were conducted in terrain-following mode, with the UAV referencing the National Land Survey (NLS) 2 m DEM to maintain altitudes of ~120 m for multispectral flights and ~ 100 m for LiDAR flights.

The multispectral flights were conducted with 70% front and 75% side overlap, yielding a 5.0 cm ground sampling distance. The multispectral data were normalised using reflectance panels and an irradiance sensor to ensure spectral consistency, while trajectory corrections were obtained in real time via the VRS network. We processed the Altum-PT images in Agisoft Metashape (version 2.0.4) using a structure-from-motion process to build ultra-high-resolution orthomosaics with ~5 cm resolution. From the spectral bands, we calculated spectral moisture and vegetation indices that are widely used in peatland and wetness studies (Table 1, Table S1). Around each WT measurement point, we created 15 cm radius buffers and extracted area-weighted averages of the spectral bands and indices (Table 2).

LiDAR data were acquired with a YellowScan Mapper+ laser scanner equipped with an Applanix APX-15 IMU, operating at a 70.4° scanning angle and 240 kHz pulse rate. The LiDAR flights were conducted at a speed of 7–8 m/s, and 55% line overlap. The resulting point density was ~385 pulses $m^{-2}$ in Välisuo and ~ 400 pulses $m^{-2}$ in Matorovansuo. Trajectory corrections were applied using Applanix POSPac with Trimnet VRS data. Preprocessing in YellowScan CloudStation v2.4 included classification of ground and non-ground points, followed by rasterization into digital terrain models (DTMs) and digital surface models (DSMs) at 20 cm resolution.

### 2.3. Processing satellite images

We used Google Earth Engine (Gorelick et al., 2017) to access and process Sentinel-2 Level-2 A surface reflectance product from the growing seasons of 2017–2023 for Lettosuo. First, we filtered out all images with >30% cloud cover. Then, we applied a cloud and cloud-shadow mask using CloudScore+ product, which has outperformed other cloud-masking algorithms (Pasquarella et al., 2023). We used a threshold value of 0.7 on the CloudScore+ cs_cdf layer, which effectively masked clouds and shadows while preserving most of the good quality pixels. To mask pixels with snow cover during the growing seasons, we used the Scene Land Cover classification provided within the Sentinel-2 product.

We used all Sentinel-2 spectral bands available at 10 and 20 m spatial resolutions (Table 2). From these bands, we also calculated a set of spectral indices (Table 2, Table S1). Finally, we constructed a 15 m radius buffer around each logger location in Lettosuo, from which we calculated area-weighted averages of the processed Sentinel-2 data. We conducted additional quality filtering of the downloaded observations by removing obvious outliers (shortwave infrared transformed reflectance (STR) < 10, Normalised Difference Vegetation Index (NDVI) < 0, Enhanced Vegetation Index (EVI) outside the −1–1 range). Additionally, we included only observation dates that provided valid data for all loggers, further reducing the influence of clouds that may have passed the earlier filters. After all filtering, we used data from 88 Sentinel-2 images in our WT analysis.

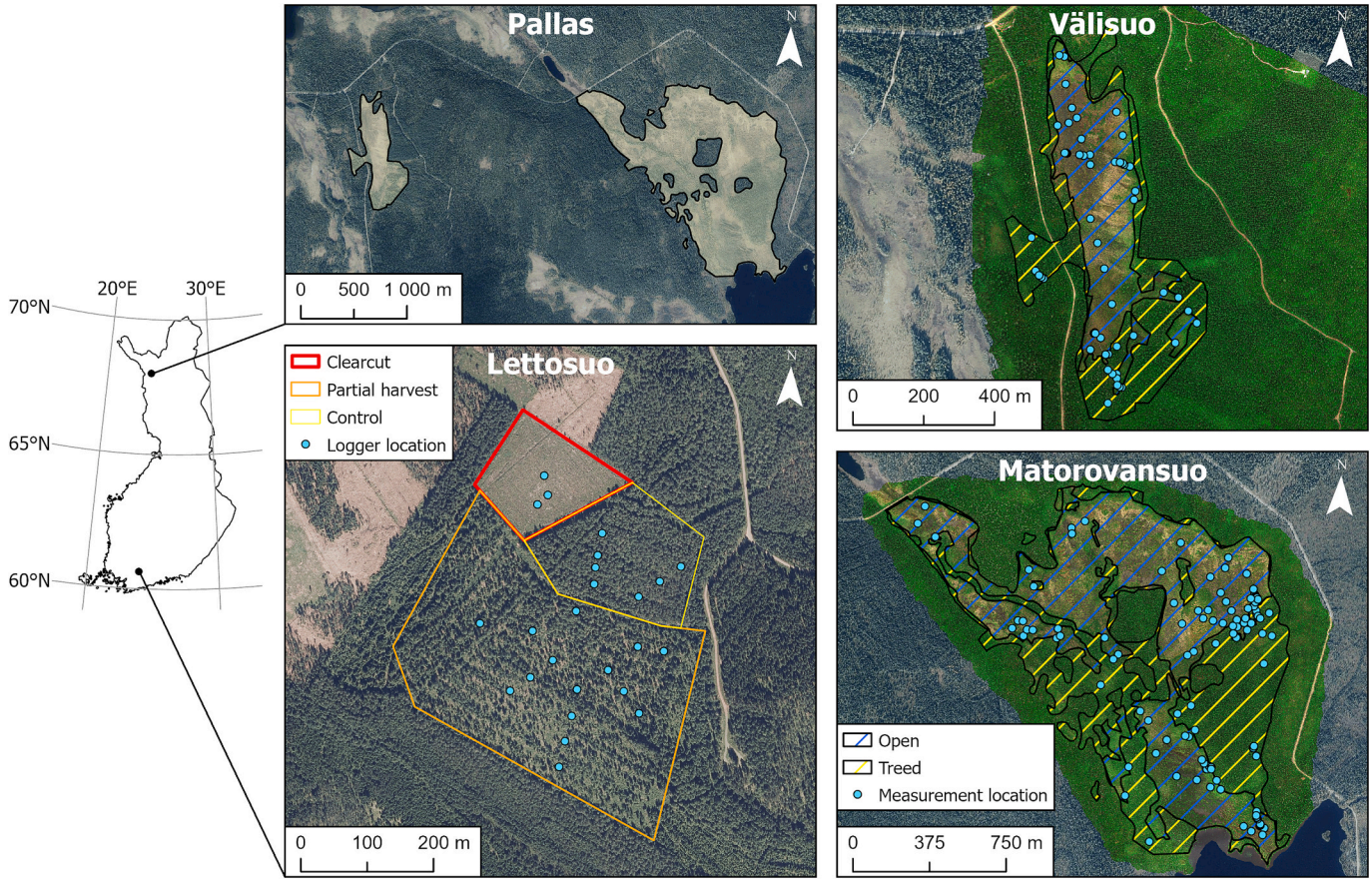


**Fig. 1.** Study site locations in Finland, manual water table measurement locations in Pallas (Matorovansuo and Välisuo), and logger locations in Lettosuo. Background aerial images for the Pallas region and Lettosuo are open data provided by the National Land Survey of Finland. Background images for Matorovansuo and Välisuo are RGB composites derived from MicaSense Altum-PT orthomosaics (see Section 2.2).

### 2.4. Environmental variables

We quantified several LiDAR-derived environmental variables from our study sites (Table 3, Table S1). For Pallas, we constructed a UAV-LiDAR-based canopy height model (CHM) by subtracting DTM from the DSM. We resampled Pallas CHM to 1 m resolution using averaging after which we applied a 3-cell-radius average filter to capture a more general CHM around the manual WT measurement locations. For Lettosuo, we used a 1 m resolution CHM from Finnish Forest Centre which was calculated from the 0.5 points $m^{-2}$ airborne LiDAR data by the National Land Survey of Finland from 2019.

From the DTM, we calculated the SAGA wetness index (SWI; Böhner and Selige, 2006), a widely used topographic wetness index, using the following parameters from Ikkala et al. (2022): suction of 256, minimum slope of 0, offset slope of 0.1, and slope weighting of 1. To reduce noise and smooth local variations in SWI, we applied a 5-cell radius median filter. We calculated slope and aspect using a 3 × 3 cell neighbourhood, and the topographic position index (TPI; Guisan et al., 1999; Weiss, 2011) using circular neighbourhood with radii of 5 and 10 m. For Pallas, we calculated depth to water (DTW; Murphy et al., 2009) index from the UAV-derived DTM using D8 stream network initiation thresholds of 0.5, 1, 2, 4, and 10 ha. For Lettosuo, we obtained DTW with identical initiation thresholds from the Natural Resources Institute Finland (Salmivaara, 2023). Finally, we calculated the planar distance to the closest drainage (DTD) from each measurement point using drainage network data from the National Land Survey of Finland. We extracted all environmental variables using the same buffers as for the optical data: 15 cm radius for Pallas and 15 m for Lettosuo.

### 2.5. Statistical analyses

We used random forest regression (Breiman, 2001) to model WT in both study regions using remote sensing variables as predictors. We built separate models for Pallas and Lettosuo with different treatments and datasets. First, we separated Pallas for treed and open areas, and Lettosuo for clearcut, control and partial cut areas (Fig. 1). Second, for each treatment we constructed models with optical data only (UAV and SAT, for Pallas and Lettosuo, respectively), and optical data with environmental variables (UAV-ENV and SAT-ENV). We also conducted site-specific models with combined data from all treatments using same dataset separations (Table 4). In total, we had 14 different model combinations.

Prior to implementing the models, we applied the Variable Selection Using Random Forests (VSURF) algorithm (Genuer et al., 2015) to select the most relevant predictors for modelling the WT. VSURF utilizes a three-step procedure (thresholding, interpretation, and prediction) with nested random forest models and variable importance metrics to remove irrelevant and redundant variables from the dataset. We repeated the VSURF procedure 10 times and retained all predictors selected in at least one iteration. This procedure aims to increase model robustness and has previously improved performance in remote sensing-based modelling (Putkiranta et al., 2024).

We fitted all random forest models using 500 decision trees. For each model, we tuned the number of variables randomly sampled at each split (mtry) by minimizing out-of-bag error using the tuneRF function from the randomForest package in R (Kuhn, 2008). We evaluated model performance using spatially and spatiotemporally structured cross-validation approaches tailored to the data characteristics of each site. In Pallas, each measurement location contained a single WT observation. To account for spatial autocorrelation, we validated the models using spatial block cross-validation with 100 m block sizes. This block size was selected based on empirical variogram analysis of WT and a block-size sensitivity analysis, which showed stabilised model performance at block sizes ≥100 m. We randomly assigned blocks to five folds and iteratively trained the model on four folds while validating it on the remaining fold. We repeated the entire modelling and validation procedure 100 times using different random seeds to account for stochastic variability in model fitting and fold assignment.

In Lettosuo, we collected repeated WT measurements over multiple years at the same locations, while environmental predictors remained temporally constant. To account for this spatiotemporal dependency and avoid information leakage, we applied a strict spatiotemporal cross-validation strategy. We defined test folds as the interaction between plot identity and year, while the training data consisted of all other plots and years. This approach ensured that no information from the same plot and the same year was present in the training set when predicting the test fold. We repeated the entire cross-validation procedure 10 times using different random seeds to account for stochastic variability in model fitting.

We quantified model performance using the coefficient of determination ($R^2$), calculated as the squared Pearson correlation coefficient between observed and predicted WT values, and the root mean square error (RMSE). We averaged performance metrics across validation folds and repeated runs. To assess predictor contributions, we extracted random forest variable importance scores from each model run, aggregated them across folds and repetitions, and calculated mean importance values for each predictor.

We upscaled spatial WT estimates for our study sites using the trained models. Before upscaling, we masked human-made objects, such as roads and duckboards, from the Pallas sites. For upscaling purposes, we resampled all optical and environmental variables to 1 m spatial resolution in Pallas and to 10 m resolution in Lettosuo. For Lettosuo, we performed upscaling using manually selected, cloud-free Sentinel-2 images from early summer (18 May 2019), midsummer (15 July 2018), and autumn (10 September 2019). We selected these dates to evaluate whether the models could capture spatiotemporal variation in WT throughout the growing season.

We examined the marginal effects of predictors on the response using partial dependence plots (PDPs). For each random forest model, we calculated PDPs with the pdp package (Greenwell, 2016) in R on a regular grid of predictor values, while averaging over the remaining variables. To obtain ensemble-level PDPs, we combined the results from all models: for each predictor, predictions were aligned to a common grid and summarized as the mean effect with 95% intervals across models.

**Table 1**
The minimum, median, maximum, and standard deviation of the measured water table by study site and treatment.

| Location | Area type / treatment | Measured water table level (cm) | | | | |
|---|---|---|---|---|---|---|
| | | Minimum | Median | Maximum | Standard deviation | Number of measurements |
| Pallas | Combined | −78 | −7 | 13 | 15.1 | 169 |
| Pallas | Open | −78 | −3 | 13 | 13.8 | 97 |
| Pallas | Treed | −60 | −19 | 5 | 14.0 | 72 |
| Lettosuo | Combined | −87.8 | −38.1 | 1.3 | 18.1 | 1731 from 25 stations |
| Lettosuo | Clearcut | −64.1 | −43.9 | −25.4 | 7.8 | 201 from 3 stations |
| Lettosuo | Control | −87.8 | −51.0 | −7.1 | 17.1 | 507 from 7 stations |
| Lettosuo | Partial cut | −73.6 | −30.1 | 1.3 | 15.8 | 1023 from 15 stations |

**Table 2**
Spectral bands and indices used in this study, their equations, and their sources (uncrewed aerial vehicle [UAV] or satellite imagery).

| Variable | Abbreviation | Equation | Reference | UAV/Satellite |
|---|---|---|---|---|
| Blue reflectance | BLUE | | | Both |
| Green reflectance | GREEN | | | Both |
| Red reflectance | RED | | | Both |
| Red edge reflectance | RE | | | UAV |
| Red edge 1 reflectance | RE1 | | | Satellite |
| Red edge 2 reflectance | RE2 | | | Satellite |
| Red edge 3 reflectance | RE3 | | | Satellite |
| Red edge 4 reflectance | RE4 | | | Satellite |
| Near-infrared reflectance | NIR | | | Both |
| Shortwave infrared band 1 reflectance | SWIR1 | | | Satellite |
| Shortwave infrared band 2 reflectance | SWIR2 | | | Satellite |
| Shortwave infrared transformed reflectance | STR | $\frac{(1-SWIR1)^2}{2\times SWIR1}$ | Sadeghi et al., 2015 | Satellite |
| Enhanced Vegetation Index | EVI | $2.5\times\frac{(NIR-RED)}{(NIR+6\times RED-7.5\times BLUE+1)}$ | Liu and Huete, 1995 | Both |
| Green Difference Vegetation Index | GDVI | $NIR-GREEN$ | Sripada et al., 2006 | Both |
| Green Normalised Difference Vegetation Index | GNDVI | $\frac{NIR-GREEN}{NIR+GREEN}$ | Gitelson et al., 1996 | Both |
| Normalised Difference Red Edge Index | NDRE | $\frac{NIR-RE}{NIR+RE}$ | Sims and Gamon, 2002 | Both |
| Normalised Difference Vegetation Index | NDVI | $\frac{NIR-RED}{NIR+RED}$ | Tucker, 1979 | Both |
| Soil Adjusted Vegetation Index | SAVI | $\left(\frac{NIR-RED}{NIR+RED+0.5}\right)\times(1+0.5)$ | Huete, 1988 | Both |
| Modified Normalised Difference Water Index | MNDWI | $\frac{Green-SWIR2}{GREEN+SWIR2}$ | H. Xu, 2006 | Satellite |
| Moisture Stress Index | MSI | $\frac{SWIR1}{NIR}$ | Hunt and Rock, 1989 | Satellite |
| Normalised Difference Moisture Index | NDMI | $\frac{NIR-SWIR1}{NIR+SWIR1}$ | Gao, 1996 | Satellite |
| Normalised Difference Moisture Index 2 | NDMI2 | $\frac{NIR-SWIR2}{NIR+SWIR2}$ | Gao, 1996 | Satellite |
| Normalised Difference Water Index | NDWI | $\frac{GREEN-NIR}{GREEN+NIR}$ | McFeeters, 1996 | Both |

## 3. Results

### 3.1. Water table modelling performances

Modelling performance ranged from relatively poor to moderate across sites and area types (Fig. 2), with $R^2$ values between 0.16 and 0.59 and RMSE ranging from 8.26 to 16.71 cm. The inclusion of environmental variables consistently improved model performance, increasing $R^2$ by 0.01–0.19 and reducing RMSE by 0.31–4.51 cm across all cases. In Pallas, UAV-ENV models produced nearly identical $R^2$ values in open and treed areas (0.41 and 0.42). In Lettosuo, the magnitude of improvement resulting from incorporating environmental variables varied by area type. The highest $R^2$ was observed in the control area, where $R^2$ increased from 0.49 to 0.59 and RMSE decreased substantially from 16.71 to 12.19 cm. In contrast, the clearcut areas showed only minor improvements ($R^2$: 0.16 to 0.17; RMSE: 8.57 to 8.26 cm).

The upscaled WT maps in Pallas showed high spatial heterogeneity in WT (Fig. 3). Strings showed lower WT values compared to the wetter flarks. Additionally, the treed area appeared drier than the open area. UAV-ENV models showed lower WT values and higher spatial heterogeneity in treed areas than the UAV models.

Upscaled WT maps for Lettosuo showed temporal and spatial variability (Fig. 4). Across all seasons, WT in the control area was consistently the lowest, while WT in the partial cut and clearcut areas was higher. This pattern was consistent in both the combined and area-specific modelling approaches. Temporal variation was also evident: WT generally decreased from early summer to midsummer and autumn. Including environmental variables (SAT-ENV models) increased spatial heterogeneity in the WT maps compared to SAT models, particularly during midsummer and autumn. Furthermore, the area-specific models showed slightly enhanced spatial differentiation among the different treatments compared to the combined model.

### 3.2. Variable importance

In Pallas, NDVI was the most important variable in the combined area model (Fig. 5a), SWI in treed area model (Fig. S2), and SAVI in the open area model (Fig. S3). In all UAV-ENV models, variables from both environmental and UAV data were selected for the final models. Of the optical variables, vegetation indices (NDVI, SAVI, GDVI, EVI), spectral bands (NIR, BLUE, RED), and NDWI were among the most important (Figs. 5a, S1, S2). Among the most important variables, SWI showed positive dependence on WT, with higher values associated with higher WT. In contrast, the dependence was opposite for TPI and vegetation indices (Figs. 5a, S1, S2), while spectral bands showed nonlinear dependence (Figs. 5a, S1, S2).

In Lettosuo, CHM was the most important variable in all SAT-ENV models (Figs. 5b, S5), except in the clearcut and control area (Figs. S3, S4). Other environmental variables (Aspect, TPI_5m, Slope, DTW, and SWI) were also among the most important predictors. From the satellite-derived variables, vegetation indices (NDVI, NDRE, SAVI), spectral bands (BLUE, RED, RE2, RE3, RE4), and moisture indices (NDMI2 and MNDWI) were found to be important in the models. According to the partial dependence plot in the combined area model, CHM showed a positive dependence on predicted WT up to ~3 m in height, followed by a broad plateau at intermediate heights, and a negative trend at the highest CHM values (Fig. 5b). Spectral vegetation and moisture indices were both positively and negatively related to WT, while the topography–WT relationships were less clear (Figs. 5b, S3, S4, S5).

## 4. Discussion

We have demonstrated that LiDAR-derived environmental variables improve the performance of both spatial and spatiotemporal WT models in boreal peatlands compared to models relying solely on optical UAV or satellite data. While multi-source remote sensing has been widely

**Table 3**
Used environmental variables, descriptions, sources, and resolutions.

| Variable | Description | Source and spatial resolution | |
|---|---|---|---|
| | | Pallas | Lettosuo |
| CHM | The height or distance between the ground and the top of vegetation or above ground features | UAV LiDAR, 1 m | Airborne LiDAR, NLS and Finnish Forest Centre, 1 m |
| SWI | An improved topographic wetness index that uses a modified catchment area calculation to predict wetness potential in flat areas more accurately | DTM (UAV-LiDAR), 1 m | DTM (NLS airborne LiDAR), 2 m |
| Slope | The steepness or gradient of a terrain surface | DTM (UAV LiDAR), 1 m | DTM (NLS airborne LiDAR), 2 m |
| Aspect | The directional orientation of the slope | DTM (UAV LiDAR), 1 m | DTM (NLS airborne LiDAR), 2 m |
| TPI | The difference between the elevation of each terrain cell and the average elevation of its surrounding cells, calculated with 5 and 10 m neighbourhood radiuses | DTM (UAV LiDAR), 1 m | DTM (NLS airborne LiDAR), 2 m |
| DTD | Planar distance from each measurement point to the nearest ditch | Topographic database (NLS) | Topographic database (NLS) |
| DTW | Cumulative slope to the nearest modelled stream, initiated with 0.5, 1, 2, 4 and 10 ha upslope contributing areas | DTM (UAV LiDAR), 1 m | Luke, 2 m (calculated from NLS 2 m DTM) |

UAV is uncrewed aerial vehicle; CHM is Canopy height model; DEM is Digital elevation model; DSM is Digital surface model; DTD is Distance to drainage; DTW is Depth to Water; DTM is Digital terrain model; NLS is National Land Survey of Finland; SWI is SAGA wetness index; TPI is Topographic position index; Luke is Natural Resources Institute Finland.

**Table 4**
Modelling set-up by site, area type/treatment, and dataset used. UAV refers to uncrewed aerial vehicle data, SAT refers to satellite data, and ENV refers to environmental data.

| Site | Area type / treatment | Datasets |
|---|---|---|
| Pallas | Combined (all areas)<br>Treed<br>Open | UAV; UAV-ENV |
| Lettosuo | Combined (all treatments)<br>Clearcut<br>Control<br>Partial Cut | SAT; SAT-ENV |

applied in peatland vegetation and greenhouse gas studies (Räsänen et al., 2020; Koch et al., 2023; Koupaei-Abyazani et al., 2024), our findings demonstrate its effectiveness for WT modelling. By combining high-resolution UAV imagery or multi-year satellite observations with LiDAR-based environmental variables, we were able to model WT patterns with relatively good performance.

Previous studies have explored UAV- and satellite-based spatial WT mapping (Lendzioch et al., 2021; Isoaho et al., 2023, 2024; Rahman et al., 2017), but to our knowledge, only a few have used a dataset as comprehensive as ours — including manual measurements, logger data, and a diverse range of remote sensing and environmental variables (Koch et al., 2023; Reddin et al., 2025). Our results further show that models incorporating environmental variables performed better than UAV- or satellite-only models in monitoring WT dynamics in treed peatland areas, which has been a major challenge in previous studies (Räsänen et al., 2022; Burdun et al., 2023).

### 4.1. Modelling performance across areas

Based on our results, the performance of WT models varied by location, area type, and variable set. This is not surprising, as earlier studies have also reported high between-site variation in the modelling performance of peatland WT (Räsänen et al., 2022; Burdun et al., 2023).

The differences in modelling performance partly reflect fundamental differences in the temporal availability of the WT datasets. In general, the models had higher $R^2$ in the Lettosuo peatland forest site than in the Pallas aapa mire site. The logger dataset from Lettosuo spans multiple years and growing seasons, whereas the Pallas dataset is based on a single WT measurement at the peak of the 2023 growing season. Therefore, the Lettosuo WT data is more comprehensive and captures both spatial and temporal variation which may be beneficial when detecting WT patterns with remote sensing. Nevertheless, the range of observed WT values is relatively similar between the study sites (Table 1).

At Pallas, the UAV model without environmental variables showed lower accuracy in treed areas compared to combined and open areas. This is expected, likely due to the dense canopy cover limiting the effectiveness of optical remote sensing in detecting surface moisture and ground vegetation signals (Burdun et al., 2023). Nevertheless, the inclusion of environmental variables (particularly topographic variables such as SWI, DTW, and TPI; Fig. S1) in the treed area boosted modelling performance such that UAV-ENV models had similar performance in open and treed areas. This highlights the role of environmental variables in compensating for the limitations of optical data under dense canopy cover.

The models in Lettosuo showed more diverse performance across different harvesting treatments, in which the densely treed control area produced the highest $R^2$ but also the highest RMSE. This may be due to the more structurally complex vegetation in control areas, which captures a broader range of WT conditions but also introduces more modelling uncertainty. The clearcut area had the lowest $R^2$ and RMSE, which was probably caused by the narrower range of observed WT compared to other areas (Table 1). Additionally, the inclusion of environmental variables did not meaningfully improve WT model performance in the clearcut area ($R^2$ increase from 0.16 to 0.17). One plausible reason is that in the absence of trees and substantial microtopography, temporally constant environmental predictors provided very little additional information. The clearcut area also contained only three WT measurement points, which is insufficient for the model to learn the behaviour of temporally constant spatial predictors. Future studies could utilise more sampling points in such areas to improve model generalisability and better capture the spatial variability of WT in post-harvest peatland environments.

### 4.2. Role of optical variables

Spectral bands and indices provided complementary information to environmental predictors at both sites. Phenological development during the summer season affects optical reflectance and thus the detectability of WT from Sentinel-2 data. Vegetation greenness and canopy density increase from early to mid-summer, leading to higher NIR reflectance and vegetation index values, which typically peak at the height of the growing season and may stabilise or decline toward late summer.

In Pallas, vegetation and moisture indices (e.g., SAVI, NDVI, GDVI, EVI, NDWI) and reflectance bands (BLUE, RED, NIR) were among the most important predictors (Fig. 5a; Figs. S1–S2). The PDPs showed a negative dependence between vegetation indices and WT, indicating that higher vegetation greenness and productivity were associated with lower WT. This pattern aligns with peatland ecology: lower WT enables the growth of vascular plants, whereas higher WT restricts vascular plants but favours mosses such as *Sphagnum* (Bengtsson et al., 2021; Breeuwer et al., 2009). The PDPs for NDWI and WT also showed a logical

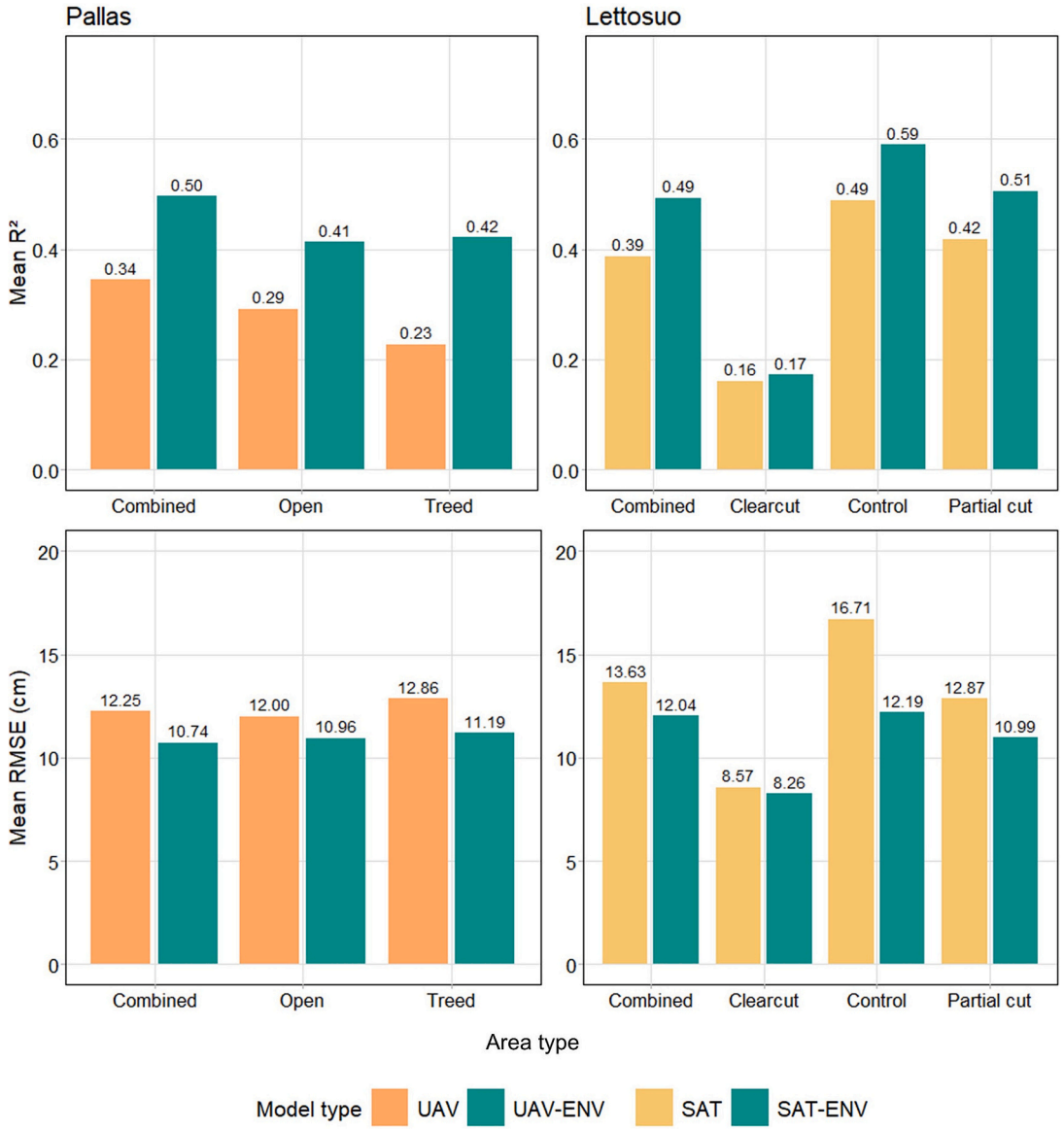


**Fig. 2.** Mean $R^2$ and RMSE from different model types in Pallas and Lettosuo. UAV refers to uncrewed aerial vehicle data, SAT refers to satellite data, and ENV refers to environmental data.

response. In the treed area model, higher NDWI values corresponded to higher WT (i.e., wetter conditions), but the response was non-linear and plateaued at around −16 cm. This reflects the fact that once soils and vegetation are already highly saturated, further increases in WT become less detectable with NDWI.

In Lettosuo, spectral variables similar to those in Pallas were also identified as important in the combined, control, and partial cut areas. However, their patterns in PDPs were less clear than in Pallas. For example, WT showed a non-linear dependency with NDVI (a vegetation greenness index) across all areas. In addition, in the combined, control, and partial cut areas, lower WT was associated with higher NDMI2 (a moisture index), although this relationship was also non-linear. WT appeared to plateau up to NDMI2 values of approximately 0.4–0.5, after which WT declined with increasing NDMI2. These unexpected patterns may be due to tree cover and data resolution. Unlike in Pallas, where high-resolution UAV data capture ground vegetation in detail, the Lettosuo analyses relied on Sentinel-2 imagery with coarser spatial resolution (10 m), which averages canopy and understory reflectance within a single pixel.

### 4.3. Role of environmental variables

Different environmental variables showed high importance across the different models. In Pallas aapa mires, topographic variables in particular were deemed important, whereas in the southern boreal peatland forest of Lettosuo, CHM was also among the most important variables.

The importance of SWI in Pallas is consistent with Ikkala et al. (2022) but not with Isoaho et al. (2023). Theoretically, SWI should capture wetness as it is based on topographic modelling of water flow routes and terrain flatness (Böhner and Selige, 2006), supporting our findings in Pallas where the relationship between SWI and WT was positive. Our sites in Pallas had greater elevation differences than the sites in the study by Isoaho et al. (2023), typical of northern aapa mires (Laitinen et al., 2007), which can affect the relative importance of SWI and its functionality in modelling wetness gradients. Finally, unlike Isoaho et al. (2023), who derived DTM from structure-from-motion photogrammetry, we calculated DTM from LiDAR point clouds, which generally produce more reliable terrain models (e.g., Alex et al., 2020). Nevertheless, in Lettosuo, the relative importance of SWI was lower than in

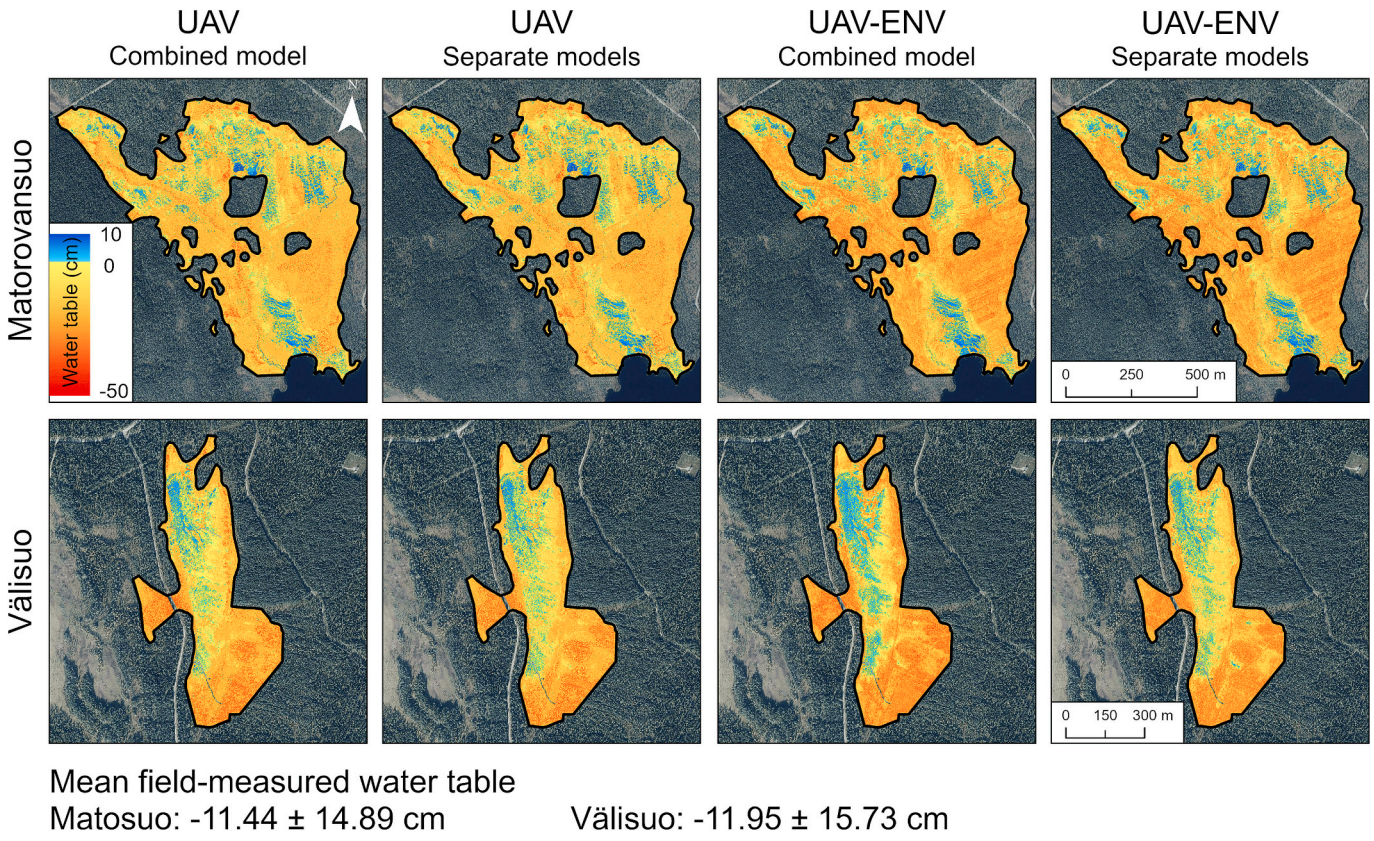


**Fig. 3.** Spatially upscaled water tables in the Pallas region. The maps were generated using different modelling approaches: optical UAV data only (columns 1–2) versus optical UAV data complemented with environmental (ENV) data (columns 3–4), with either combined models for all areas or separate models for open and treed peatlands. UAV refers to uncrewed aerial vehicle data.

Pallas, which may be attributed to the flatness of the site and the high importance of CHM.

CHM emerged as a key predictor in the spatiotemporal SAT-ENV models in Lettosuo. In the combined model, CHM's importance was the strongest, likely because it helps to distinguish between treeless and treed areas, where WT values differ. In addition, CHM was also the most important variable in the partial cut area. The importance of CHM can be attributed to its role as a proxy for forest structure and stand volume, both of which directly influence evapotranspiration rates. Previous studies have demonstrated that WT is highly dependent on stand volume, with evapotranspiration from mature and denser tree stands acting as a key regulator of WT during the growing season (Hökkä et al., 2008; Sarkkola et al., 2010, 2013). As such, CHM serves not only as an indicator of canopy presence but also indirectly captures the hydrological impact of vegetation on peatland water dynamics. In Pallas, CHM did not emerge as an important predictor because tree cover is sparse, and WT variation is primarily controlled by macro- and microtopographical patterns that are characteristic of aapa mires (Laitinen et al., 2007; Maanavilja et al., 2011).

DTW was selected in most models, except in the Lettosuo combined and clearcut areas. DTW represents the cumulative slope from the ground surface to the nearest modelled stream and therefore integrates terrain configuration, flow accumulation, and water flow networks (Murphy et al., 2009) into a single hydrologically meaningful predictor (Ågren et al., 2021; Larson et al., 2022). Unlike purely local wetness indices, DTW captures broader landscape-scale controls on subsurface water availability and has been shown to perform well as a predictor of soil moisture and groundwater conditions in boreal forested environments (Ågren et al., 2021; Rahman et al., 2017). In theory, high DTW values should be associated with WT deep below the ground surface and low DTW values with WT close to the surface; however, in our case, this relationship was observed only for DTW with a 0.5 ha stream network initiation threshold in the Pallas open and combined area models.

Our Pallas models also showed the importance of TPI, which has not been reported previously in GIS- or remote sensing-based WT modelling. TPI helps to characterise the relative location of a point—with a positive TPI indicating an elevated position compared to its neighbouring area—which is a known determinant of water accumulation (Lendzioch et al., 2021; Rinderer et al., 2014). TPI, measured at both 5 and 10 m neighbourhood distances, had a negative relationship with WT. Negative TPI was linked with high and relatively constant WT, whereas higher TPI was linked to lower WT. This relationship is consistent with WT being naturally lower in elevated strings than in flat flarks (Heiskanen et al., 2021; Maanavilja et al., 2011). However, TPI was less important in Lettosuo, where flatter terrain, efficient drainage, and strong stand-related effects (e.g., drier areas under dense canopies versus wetter clearcuts) likely reduced the role of topography in shaping WT.

In the Pallas combined area, DTD showed a clear threshold response, with higher WT levels beyond ~50 m from a ditch. This pattern is consistent with Nimr et al. (2026), who showed that immediate restoration effect on peatland WT was around same distance. Furthermore and it somewhat matches the dense ditch spacing needed for effective drainage (Nieminen et al., 2018). However, DTD was selected in only one out of seven models in the iterative VSURF procedure. This is likely because WT variation in other areas was more strongly explained by other environmental variables than by DTD. In addition, in Lettosuo, all loggers were located within 35 m of a ditch, limiting the detectable range of DTD effects on WT. Additionally, the impact of DTD on WT is strongly affected by the humification degree of peat, as hydraulic conductivity decreases strongly with higher humification (Päivänen, 1969).

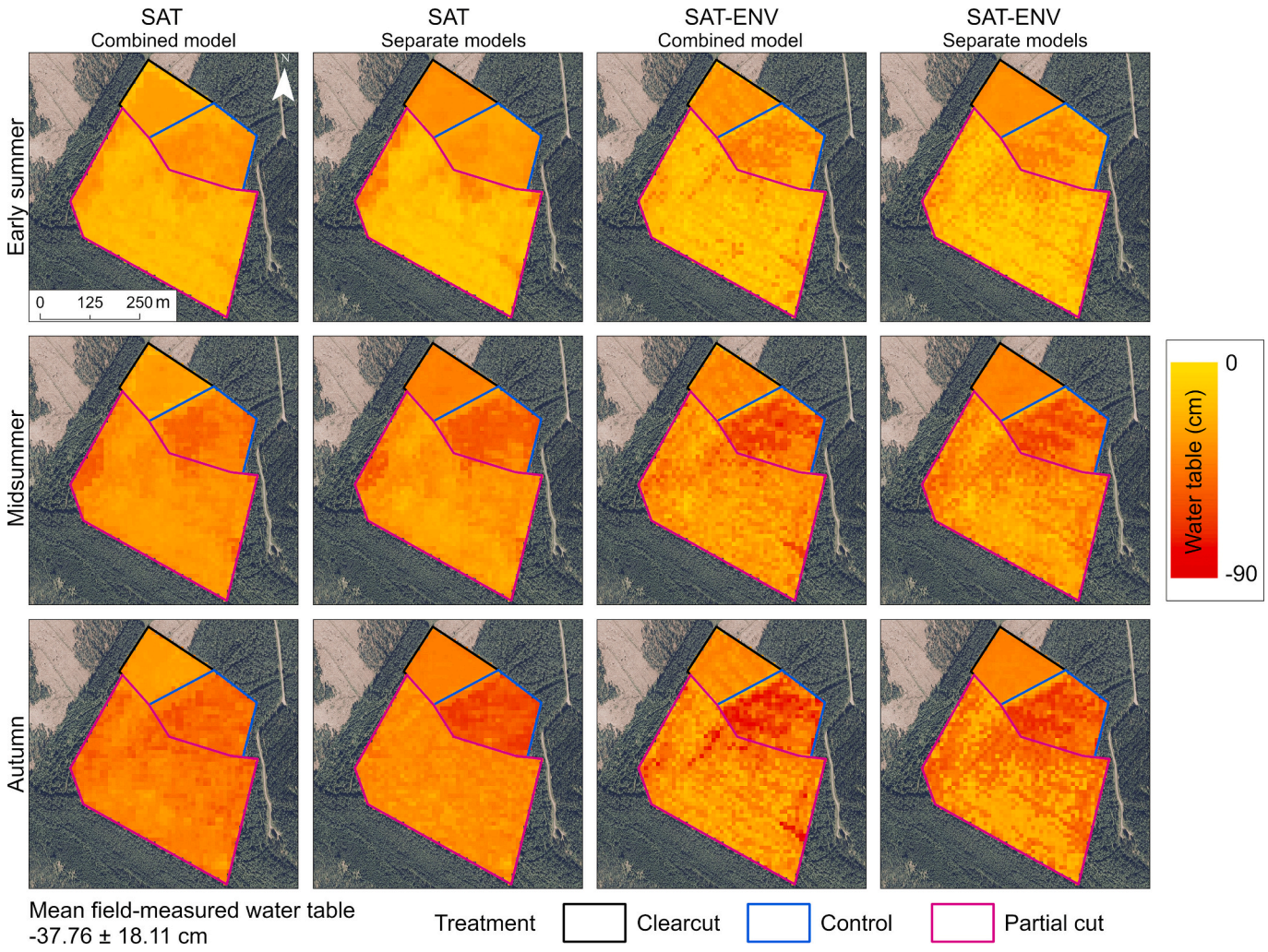


**Fig. 4.** Spatially upscaled water tables in Lettosuo across three seasonal periods (early summer, midsummer, and autumn), generated using optical satellite (SAT) data and SAT data complemented with environmental (SAT-ENV) data with combined models for all areas or separate models for the different treatments (clearcut, control, partial cut).

### *4.4. Study limitations*

Our study has several limitations that also point to directions for future research. First, environmental variables such as SWI, TPI, DTW, and CHM were static in time and therefore could not capture short-term hydrological dynamics. Future studies could thus also include temporally dynamic environmental variables. Second, WT measurements in Pallas represent a single time point, which limits temporal generalisation and underscores the need for repeated field measurements to better capture seasonal and interannual variability. Third, sampling near drainage features was sparse, reducing the model's ability to learn distance-based drainage effects; denser WT sampling along ditches would help address this limitation. Finally, the transferability of the models to other peatland types or climatic regions remains uncertain and should be evaluated through cross-site validation. Because patterned aapa mires share broadly similar macro- and microtopographic structures across northern Fennoscandia, the strong influence of topographic variables observed in Pallas is likely applicable to other aapa mire systems. However, site-specific drainage histories and vegetation structure — such as the distribution of plant functional types across strings and flarks, shrub and tree cover, and canopy density — may still influence model performance and should be taken into account in future studies.

### *4.5. Implications for peatland monitoring and restoration*

Spatially continuous WT information is essential for planning peatland restoration and monitoring its outcomes; therefore, the multi-source remote sensing approach demonstrated in this study offers a scalable alternative, with relevance in the context of current management, conservation, and restoration policies. For example, the EU Nature Restoration Regulation requires member states to conduct large-scale restoration actions in various ecosystem and habitat types, including wetlands, and rewet drained peatlands. Similarly, the EU Biodiversity Strategy 2030 and the global Kunming-Montreal Framework both require verifiable restoration outcomes. Tracking progress toward these targets demands spatially explicit, temporally repeated WT monitoring—a need that remote sensing-based models complemented with environmental variables could help to address. The upscaled WT maps generated with the methods described here could therefore support restoration planning and post-intervention evaluation, though their utility depends on the availability of site-specific calibration data and the transferability of models to new sites.

## 5. Conclusions

Our study demonstrates that multi-source remote sensing—especially the combination of optical UAV or satellite variables

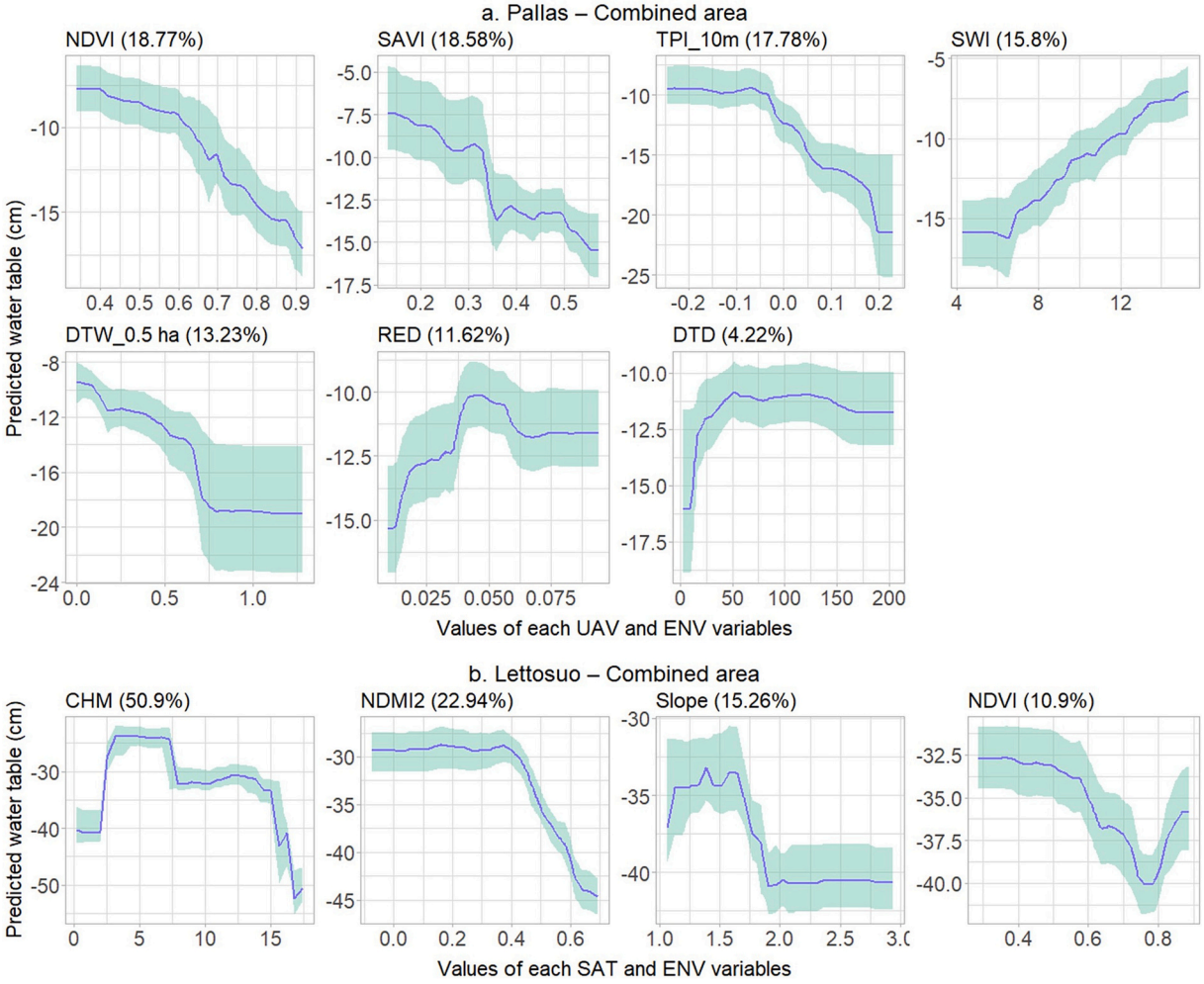


**Fig. 5.** Partial dependence plots for selected predictors in the combined areas of (a) Pallas and (b) Lettosuo. The plots show the marginal effect of each variable on predicted water table (cm), based on the uncrewed aerial vehicle (UAV) or satellite (SAT) data models complemented with environmental (ENV) variables. The blue line shows the average relationship between each selected predictor and water table across model iterations, indicating how changes in selected predictor values are associated with increases or decreases in water table. The shaded green area represents the 95% confidence interval. The value in parentheses next to each subplot title shows the relative variable importance of each predictor to the model. For variable abbreviations, refer to Tables 2 and 3.

with LiDAR-derived environmental variables—can effectively model and capture spatial and spatiotemporal WT dynamics in boreal peatlands. Notably, the inclusion of environmental variables improves WT prediction compared to models relying on optical variables only. Nevertheless, the environmental variables with the strongest effect differ between sites. Topographic environmental variables substantially improved spatial WT models in the patterned northern aapa mires of Pallas. In the drained peatland forest of Lettosuo, spatiotemporal WT prediction was further improved by the inclusion of tree-stand structure information. These results imply that multi-source remote sensing offers an efficient and scalable approach for monitoring WT across large or remote peatland areas and can therefore assist evidence-based decision-making in peatland conservation and climate mitigation efforts. Accurate spatial and temporal WT information is essential for assessing drainage impacts and monitoring restoration outcomes, which supports the implementation of instruments such as the EU Nature Restoration Regulation.

## CRediT authorship contribution statement

**Priscillia Christiani:** Writing – original draft, Visualization, Validation, Software, Methodology, Investigation, Formal analysis. **Aleksi Räsänen:** Writing – review & editing, Investigation, Funding acquisition, Conceptualization. **Anton Kuzmin:** Investigation, Data curation. **Paavo Ojanen:** Writing – review & editing, Data curation. **Kari Minkkinen:** Writing – review & editing, Data curation. **Pasi Korpelainen:** Investigation, Data curation. **Parvez Rana:** Writing – review & editing, Investigation, Funding acquisition, Data curation. **Timo Kumpula:** Writing – review & editing. **Aleksi Isoaho:** Writing – review & editing, Writing – original draft, Visualization, Methodology, Investigation, Data curation, Conceptualization.

## Declaration of competing interest

The authors declare that they have no known competing financial interests or personal relationships that could have appeared to influence the work reported in this paper.

## Acknowledgements

This study was funded by European Union LIFE programme (LIFE21-CCM-LV-LIFE-PeatCarbon, LIFE22-IPN-FI-Priodiversity LIFE), Horizon programme project ALFAwetlands (Grant Agreement Number 101056844), and Kone Foundation. We thank Kaapro Keränen for assisting in the field work.

## Appendix A. Supplementary data

Supplementary data to this article can be found online at https://doi.org/10.1016/j.scitotenv.2026.182017.

## Data availability

Data will be made available on request.

## References


Ågren, A.M., Larson, J., Paul, S.S., Laudon, H., Lidberg, W., 2021. Use of multiple LIDAR-derived digital terrain indices and machine learning for high-resolution national-scale soil moisture mapping of the Swedish forest landscape. Geoderma 404, 115280. https://doi.org/10.1016/j.geoderma.2021.115280.

Ahmad, S., Wang, M., Bates, A., Martini, F., Regan, S., Saunders, M., Liu, H., McElwain, J., Gill, L., 2025. Flatlining fens? Small-scale variations in peat properties and microtopography as indicators of ecosystem homogenisation. Ecol. Indic. 172, 113317. https://doi.org/10.1016/j.ecolind.2025.113317.

Albert-Saiz, M., Lamentowicz, M., Rastogi, A., Juszczak, R., 2025. Unveiling water table tipping points in peatland ecosystems: implications for ecological restoration. CATENA 257, 109149. https://doi.org/10.1016/j.catena.2025.109149.

Alex, M.-A., Víctor, G.-M., Jesús, Á.-M., 2020. Comparison of digital terrain models obtained with LiDAR and photogrammetry. In: Cavas-Martínez, F., Sanz-Adan, F., Morer Camo, P., Lostado Lorza, R., Santamaría Peña, J. (Eds.), Advances in Design Engineering. Springer International Publishing, pp. 576–585. https://doi.org/10.1007/978-3-030-41200-5_63.

Asmuß, T., Bechtold, M., Tiemeyer, B., 2019. On the potential of Sentinel-1 for high resolution monitoring of water table dynamics in grasslands on organic soils. Remote Sens. 11 (14), 1659. https://doi.org/10.3390/rs11141659.

Bechtold, M., Schlaffer, S., Tiemeyer, B., De Lannoy, G., 2018. Inferring water table depth dynamics from ENVISAT-ASAR C-band backscatter over a range of peatlands from deeply-drained to natural conditions. Remote Sens. 10 (4), 536. https://doi.org/10.3390/rs10040536.

Bengtsson, F., Rydin, H., Baltzer, J.L., Bragazza, L., Bu, Z., Caporn, S.J.M., Dorrepaal, E., Flatberg, K.I., Galanina, O., Gałka, M., Ganeva, A., Goia, I., Goncharova, N., Hájek, M., Haraguchi, A., Harris, L.I., Humphreys, E., Jiroušek, M., Kajukało, K., Karofeld, E., Koronatova, N.G., Kosykh, N.P., Laine, A.M., Lamentowicz, M., Lapshina, E., Limpens, J., Linkosalmi, M., Ma, J.-Z., Mauritz, M., Mitchell, E.A.D., Munir, T.M., Natali, S.M., Natcheva, R., Payne, R.J., Philippov, D.A., Rice, S.K., Robinson, S., Robroek, B.J.M., Rochefort, L., Singer, D., Stenøien, H.K., Tuittila, E.-S., Vellak, K., Waddington, J.M., Granath, G., 2021. Environmental drivers of *Sphagnum* growth in peatlands across the Holarctic region. J. Ecol. 109 (1), 417–431. https://doi.org/10.1111/1365-2745.13499.

Böhner, J., Selige, T., 2006. Spatial prediction of soil attributes using terrain analysis and climate regionalisation. Gott. Geogr. Abh. 115, 13–28.

Braekke, F.H., 1983. Water table levels at different drainage intensities on deep peat in Northern Norway. For. Ecol. Manag. 5 (3), 169–192. https://doi.org/10.1016/0378-1127(83)90070-1.

Breeuwer, A., Robroek, B.J.M., Limpens, J., Heijmans, M.M.P.D., Schouten, M.G.C., Berendse, F., 2009. Decreased summer water table depth affects peatland vegetation. Basic Appl. Ecol. 10 (4), 330–339. https://doi.org/10.1016/j.baae.2008.05.005.

Breiman, L., 2001. Random forests. Mach. Learn. 45 (1), 5–32. https://doi.org/10.1023/A:1010933404324.

Burdun, I., Bechtold, M., Aurela, M., De Lannoy, G., Desai, A.R., Humphreys, E., Kareksela, S., Komisarenko, V., Liimatainen, M., Marttila, H., Minkkinen, K., Nilsson, M.B., Ojanen, P., Salko, S.-S., Tuittila, E.-S., Uuemaa, E., Rautiainen, M., 2023. Hidden becomes clear: optical remote sensing of vegetation reveals water table dynamics in northern peatlands. Remote Sens. Environ. 296, 113736. https://doi.org/10.1016/j.rse.2023.113736.

Crockett, A.C., Ronayne, M.J., Cooper, D.J., 2016. Relationships between vegetation type, peat hydraulic conductivity, and water table dynamics in mountain fens. Ecohydrology 9 (6), 1028–1038. https://doi.org/10.1002/eco.1706.

Eurola, S., Huttunen, A., Kukko-oja, A., 1995. *Suokasvillisuusopas*. [Mire vegetation guide]. In: Oulanka Reports, 14, pp. 1–85.

Evans, C.D., Peacock, M., Baird, A.J., Artz, R.R.E., Burden, A., Callaghan, N., Chapman, P.J., Cooper, H.M., Coyle, M., Craig, E., Cumming, A., Dixon, S., Gauci, V., Grayson, R.P., Helfter, C., Heppell, C.M., Holden, J., Jones, D.L., Kaduk, J., Levy, P., Matthews, R., McNamara, N.P., Misselbrook, T., Oakley, S., Page, S.E., Rayment, M., Ridley, L.M., Stanley, K.M., Williamson, J.L., Worrall, F., Morrison, R., 2021. Overriding water table control on managed peatland greenhouse gas emissions. Nature 593 (7860), 548–552. https://doi.org/10.1038/s41586-021-03523-1.

Gao, B., 1996. NDWI—A normalized difference water index for remote sensing of vegetation liquid water from space. Remote Sens. Environ. 58 (3), 257–266. https://doi.org/10.1016/S0034-4257(96)00067-3.

Genuer, R., Poggi, J.-M., Tuleau-Malot, C., 2015. VSURF: an R package for variable selection using random forests. R J. 7 (2), 19–33.

Ghazaryan, G., Krupp, L., Seyfried, S., Landgraf, N., Nendel, C., 2024. Enhancing peatland monitoring through multisource remote sensing: optical and radar data applications. Int. J. Remote Sens. 45 (18), 6372–6394. https://doi.org/10.1080/01431161.2024.2387133.

Gitelson, A.A., Kaufman, Y.J., Merzlyak, M.N., 1996. Use of a green channel in remote sensing of global vegetation from EOS-MODIS. Remote Sens. Environ. 58 (3), 289–298. https://doi.org/10.1016/S0034-4257(96)00072-7.

Gorelick, N., Hancher, M., Dixon, M., Ilyushchenko, S., Thau, D., Moore, R., 2017. Google Earth Engine: planetary-scale geospatial analysis for everyone. Remote Sens. Environ. 202, 18–27. https://doi.org/10.1016/j.rse.2017.06.031.

Greenwell, B.M., 2016. pdp: Partial Dependence Plots (p. 0.8.2) [Dataset]. https://doi.org/10.32614/CRAN.package.pdp.

Guisan, A., Weiss, S.B., Weiss, A.D., 1999. GLM versus CCA spatial modeling of plant species distribution. Plant Ecol. 143 (1), 107–122. https://doi.org/10.1023/A:1009841519580.

Haapalehto, T., Kotiaho, J.S., Matilainen, R., Tahvanainen, T., 2014. The effects of long-term drainage and subsequent restoration on water table level and pore water chemistry in boreal peatlands. J. Hydrol. 519, 1493–1505. https://doi.org/10.1016/j.jhydrol.2014.09.013.

Harris, A., Baird, A.J., 2019. Microtopographic drivers of vegetation patterning in blanket peatlands recovering from erosion. Ecosystems 22 (5), 1035–1054. https://doi.org/10.1007/s10021-018-0321-6.

Heikkinen, S., Räsänen, A., Kuzmin, A., Korpelainen, P., Kumpula, T., Isoaho, A., 2026. Downscaling satellite-derived optical trapezoid model with uncrewed aerial vehicle data for peatland water table monitoring. PFG. https://doi.org/10.1007/s41064-026-00389-8.

Heiskanen, L., Tuovinen, J.-P., Räsänen, A., Virtanen, T., Juutinen, S., Lohila, A., Penttilä, T., Linkosalmi, M., Mikola, J., Laurila, T., Aurela, M., 2021. Carbon dioxide and methane exchange of a patterned subarctic fen during two contrasting growing seasons. Biogeosciences 18 (3), 873–896. https://doi.org/10.5194/bg-18-873-2021.

Henrion, M., Li, Y., Koganti, T., Bechtold, M., Jonard, F., Opfergelt, S., Vanacker, V., Van Oost, K., Lambot, S., 2024. Mapping and monitoring peatlands in the Belgian Hautes Fagnes: insights from ground-penetrating radar and electromagnetic induction characterization. Geoderma Reg. 37, e00795. https://doi.org/10.1016/j.geodrs.2024.e00795.

Hökkä, H., Repola, J., Laine, J., 2008. Quantifying the interrelationship between tree stand growth rate and water table level in drained peatland sites within Central Finland. Can. J. For. Res. 38 (7), 1775–1783. https://doi.org/10.1139/X08-028.

Huete, A.R., 1988. A soil-adjusted vegetation index (SAVI). Remote Sens. Environ. 25 (3), 295–309. https://doi.org/10.1016/0034-4257(88)90106-X.

Hunt, E.R., Rock, B.N., 1989. Detection of changes in leaf water content using near- and middle-infrared reflectances. Remote Sens. Environ. 30 (1), 43–54. https://doi.org/10.1016/0034-4257(89)90046-1.

Ikkala, L., Ronkanen, A.-K., Ilmonen, J., Similä, M., Rehell, S., Kumpula, T., Päkkilä, L., Klöve, B., Marttila, H., 2022. Unmanned aircraft system (UAS) structure-from-motion (SfM) for monitoring the changed flow paths and wetness in minerotrophic peatland restoration. Remote Sens. 14 (13), 3169. https://doi.org/10.3390/rs14133169.

Isoaho, A., Ikkala, L., Marttila, H., Hjort, J., Kumpula, T., Korpelainen, P., Räsänen, A., 2023. Spatial water table level modelling with multi-sensor unmanned aerial vehicle data in boreal aapa mires. Remot. Sens. Appl. Soc. Environ. 32, 101059. https://doi.org/10.1016/j.rsase.2023.101059.

Isoaho, A., Ikkala, L., Päkkilä, L., Marttila, H., Kareksela, S., Räsänen, A., 2024. Multi-sensor satellite imagery reveals spatiotemporal changes in peatland water table after restoration. Remote Sens. Environ. 306, 114144. https://doi.org/10.1016/j.rse.2024.114144.

Jackson, T.J., Chen, D., Cosh, M., Li, F., Anderson, M., Walthall, C., Doriaswamy, P., Hunt, E.R., 2004. Vegetation water content mapping using Landsat data derived normalized difference water index for corn and soybeans. Remote Sens. Environ. 92 (4), 475–482. https://doi.org/10.1016/j.rse.2003.10.021.

Juutinen, A., Artell, J., Iivonen, S., Tolvanen, A., 2024. *Socio-Economic Impacts Caused by the Restoration of Peatlands and Small Water Bodies* (Natural Resources and Bioeconomy Studies 2/24). Natural Resources Institute Finland.

Kalacska, M., Arroyo-Mora, J., Soffer, R., Roulet, N., Moore, T., Humphreys, E., Leblanc, G., Lucanus, O., Inamdar, D., 2018. Estimating peatland water table depth and net ecosystem exchange: a comparison between satellite and airborne imagery. Remote Sens. 10 (5), 687. https://doi.org/10.3390/rs10050687.

Koch, J., Elsgaard, L., Greve, M.H., Gyldenkærne, S., Hermansen, C., Levin, G., Wu, S., Stisen, S., 2023. Water-table-driven greenhouse gas emission estimates guide peatland restoration at national scale. Biogeosciences 20 (12), 2387–2403. https://doi.org/10.5194/bg-20-2387-2023.

Korkiakoski, M., Ojanen, P., Tuovinen, J.-P., Minkkinen, K., Nevalainen, O., Penttilä, T., Aurela, M., Laurila, T., Lohila, A., 2023. Partial cutting of a boreal nutrient-rich peatland forest causes radically less short-term on-site CO2 emissions than clear-cutting. Agric. For. Meteorol. 332, 109361. https://doi.org/10.1016/j.agrformet.2023.109361.

Koupaei-Abyazani, N., Burdun, I., Desai, A.R., Hergoualc'h, K., Hirano, T., Melling, L., Swails, E., Ing Tang, A.C., Wong, G.X., 2024. Tropical peatland water table estimations from space. J. Geophys. Res. Biogeosci. 129 (6), e2024JG008116. https://doi.org/10.1029/2024JG008116.

Kuhn, M., 2008. Building predictive models in *R* using the caret package. J. Stat. Softw. 28 (5). https://doi.org/10.18637/jss.v028.i05.

Laitinen, J., Rehell, S., Huttunen, A., Tahvanainen, T., Heikkilä, R., Lindholm, T., 2007. Mire systems in Finland—special view to aapa mires and their water-flow pattern. Suo 58 (1), 1–26.

Larson, J., Lidberg, W., Ågren, A.M., Laudon, H., 2022. Predicting soil moisture conditions across a heterogeneous boreal catchment using terrain indices. Hydrol. Earth Syst. Sci. 26 (19), 4837–4851. https://doi.org/10.5194/hess-26-4837-2022.

Lendzioch, T., Langhammer, J., Vlček, L., Minařík, R., 2021. Mapping the groundwater level and soil moisture of a montane peat bog using UAV monitoring and machine learning. Remote Sens. 13 (5), 907. https://doi.org/10.3390/rs13050907.

Vegetation height and vertical structure. In: Liang, S., Wang, J. (Eds.), 2020. Advanced Remote Sensing. Elsevier, pp. 511–542. https://doi.org/10.1016/B978-0-12-815826-5.00013-1.

Liu, H.Q., Huete, A., 1995. A feedback based modification of the NDVI to minimize canopy background and atmospheric noise. IEEE Trans. Geosci. Remote Sens. 33 (2), 457–465. https://doi.org/10.1109/TGRS.1995.8746027.

Ma, L., Zhu, G., Chen, B., Zhang, K., Niu, S., Wang, J., Ciais, P., Zuo, H., 2022. A globally robust relationship between water table decline, subsidence rate, and carbon release from peatlands. Commun. Earth Environ. 3 (1), 254. https://doi.org/10.1038/s43247-022-00590-8.

Maanavilja, L., Riutta, T., Aurela, M., Pulkkinen, M., Laurila, T., Tuittila, E.-S., 2011. Spatial variation in CO2 exchange at a northern aapa mire. Biogeochemistry 104 (1–3), 325–345. https://doi.org/10.1007/s10533-010-9505-7.

McFeeters, S.K., 1996. The use of the Normalized Difference Water Index (NDWI) in the delineation of open water features. Int. J. Remote Sens. 17 (7), 1425–1432. https://doi.org/10.1080/01431169608948714.

Millard, K., Richardson, M., 2018. Quantifying the relative contributions of vegetation and soil moisture conditions to polarimetric C-Band SAR response in a temperate peatland. Remote Sens. Environ. 206, 123–138. https://doi.org/10.1016/j.rse.2017.12.011.

Minasny, B., Adetsu, D.V., Aitkenhead, M., Artz, R.R.E., Baggaley, N., Barthelmes, A., Beucher, A., Caron, J., Conchedda, G., Connolly, J., Deragon, R., Evans, C., Fadnes, K., Fiantis, D., Gagkas, Z., Gilet, L., Gimona, A., Glatzel, S., Greve, M.H., Habib, W., Hergoualc'h, K., Hermansen, C., Kidd, D.B., Koganti, T., Kopansky, D., Large, D.J., Larmola, T., Lilly, A., Liu, H., Marcus, M., Middleton, M., Morrison, K., Petersen, R.J., Quaife, T., Rochefort, L., Rudiyanto, Toca, Tubiello, F.N., Weber, P.L., Weldon, S., Widyatmanti, W., Williamson, J., Zak, D., 2023. Mapping and monitoring peatland conditions from global to field scale. Biogeochemistry 167 (4), 383–425. https://doi.org/10.1007/s10533-023-01084-1.

Murphy, P.N.C., Ogilvie, J., Arp, P., 2009. Topographic modelling of soil moisture conditions: a comparison and verification of two models. Eur. J. Soil Sci. 60 (1), 94–109. https://doi.org/10.1111/j.1365-2389.2008.01094.x.

Nieminen, M., Piirainen, S., Sikström, U., Löfgren, S., Marttila, H., Sarkkola, S., Laurén, A., Finér, L., 2018. Ditch network maintenance in peat-dominated boreal forests: review and analysis of water quality management options. Ambio 47 (5), 535–545. https://doi.org/10.1007/s13280-018-1047-6.

Nimr, O.A., Marttila, H., Batelaan, O., Partington, D., Ala-Aho, P., 2026. How Does Rewetting Propagate Through Restored Peatlands? An Integrated Surface–subsurface Modelling Analysis of Water–table Dynamics. SSRN. https://doi.org/10.2139/ssrn.6265631.

Päivänen, J., 1969. The bulk density of peat and its determination. Silva Fennica 3 (1). https://doi.org/10.14214/sf.a14569.

Pasquarella, V.J., Brown, C.F., Czerwinski, W., Rucklidge, W.J., 2023. Comprehensive quality assessment of optical satellite imagery using weakly supervised video learning. In: 2023 IEEE/CVF Conference on Computer Vision and Pattern Recognition Workshops (CVPRW), pp. 2125–2135. https://doi.org/10.1109/CVPRW59228.2023.00206.

Putkiranta, P., Räsänen, A., Korpelainen, P., Erlandsson, R., Kolari, T.H.M., Pang, Y., Villoslada, M., Wolff, F., Kumpula, T., Virtanen, T., 2024. The value of hyperspectral UAV imagery in characterizing tundra vegetation. Remote Sens. Environ. 308, 114175. https://doi.org/10.1016/j.rse.2024.114175.

Rahman, M.M., McDermid, G.J., Strack, M., Lovitt, J., 2017. A new method to map groundwater table in peatlands using unmanned aerial vehicles. Remote Sens. 9 (10), 1057. https://doi.org/10.3390/rs9101057.

Ramchunder, S.J., Brown, L.E., Holden, J., 2012. Catchment-scale peatland restoration benefits stream ecosystem biodiversity. J. Appl. Ecol. 49 (1), 182–191. https://doi.org/10.1111/j.1365-2664.2011.02075.x.

Räsänen, A., Aurela, M., Juutinen, S., Kumpula, T., Lohila, A., Penttilä, T., Virtanen, T., 2020. Detecting northern peatland vegetation patterns at ultra-high spatial resolution. Remot. Sens. Ecol. Conserv. 6 (4), 457–471. https://doi.org/10.1002/rse2.140.

Räsänen, A., Tolvanen, A., Kareksela, S., 2022. Monitoring peatland water table depth with optical and radar satellite imagery. Int. J. Appl. Earth Obs. Geoinf. 112, 102866. https://doi.org/10.1016/j.jag.2022.102866.

Reddin, E., Hanafin, J., Tong, M., Gill, L., Healy, M.G., 2025. Modelling water table depth at rewetted peatlands with Sentinel-1 and Sentinel-2. Sci. Remot. Sens. 11, 100238. https://doi.org/10.1016/j.srs.2025.100238.

Rinderer, M., Van Meerveld, H.J., Seibert, J., 2014. Topographic controls on shallow groundwater levels in a steep, prealpine catchment: when are the TWI assumptions valid? Water Resour. Res. 50 (7), 6067–6080. https://doi.org/10.1002/2013WR015009.

Rydin, H., Gunnarsson, U., Sundberg, S., 2006. The role of sphagnum in Peatland development and persistence. In: Wieder, R.K., Vitt, D.H. (Eds.), Boreal Peatland Ecosystems, vol. 188. Springer Berlin Heidelberg, pp. 47–65. https://doi.org/10.1007/978-3-540-31913-9_4.

Sadeghi, M., Jones, S.B., Philpot, W.D., 2015. A linear physically-based model for remote sensing of soil moisture using short wave infrared bands. Remote Sens. Environ. 164, 66–76. https://doi.org/10.1016/j.rse.2015.04.007.

Sadeghi, M., Babaeian, E., Tuller, M., Jones, S.B., 2017. The optical trapezoid model: a novel approach to remote sensing of soil moisture applied to Sentinel-2 and Landsat-8 observations. Remote Sens. Environ. 198, 52–68. https://doi.org/10.1016/j.rse.2017.05.041.

Salmivaara, A., 2023. Cartographic Depth-to-Water (DTW) index map. *2m* (Version 1) [Dataset]. CSC – IT Center for Science. http://urn.fi/urn:nbn:fi:att:770f345e-58d4-45e5-b4e7-3fdbd858872f.

Sarkkola, S., Hökkä, H., Koivusalo, H., Nieminen, M., Ahti, E., Päivänen, J., Laine, J., 2010. Role of tree stand evapotranspiration in maintaining satisfactory drainage conditions in drained peatlands. Can. J. For. Res. 40 (8), 1485–1496. https://doi.org/10.1139/X10-084.

Sarkkola, S., Nieminen, M., Koivusalo, H., Laurén, A., Ahti, E., Launiainen, S., Nikinmaa, E., Marttila, H., Laine, J., Hökkä, H., 2013. Domination of growing-season evapotranspiration over runoff makes ditch network maintenance in mature peatland forests questionable. Mires Peat 11.

Sims, D.A., Gamon, J.A., 2002. Relationships between leaf pigment content and spectral reflectance across a wide range of species, leaf structures and developmental stages. Remote Sens. Environ. 81 (2–3), 337–354. https://doi.org/10.1016/S0034-4257(02)00010-X.

Sripada, R.P., Heiniger, R.W., White, J.G., Meijer, A.D., 2006. Aerial color infrared photography for determining early in-season nitrogen requirements in corn. Agron. J. 98 (4), 968–977. https://doi.org/10.2134/agronj2005.0200.

Thompson, D.K., Waddington, J.M., 2008. *Sphagnum* under pressure: towards an ecohydrological approach to examining *Sphagnum* productivity. Ecohydrology 1 (4), 299–308. https://doi.org/10.1002/eco.31.

Trappe, J., Kneisel, C., 2019. Geophysical and sedimentological investigations of peatlands for the assessment of lithology and subsurface water pathways. Geosciences 9 (3), 118. https://doi.org/10.3390/geosciences9030118.

Tucker, C.J., 1979. Red and photographic infrared linear combinations for monitoring vegetation. Remote Sens. Environ. 8 (2), 127–150. https://doi.org/10.1016/0034-4257(79)90013-0.

Weiss, A., 2011. Topographic position and landforms analysis. In: [Poster Presentation]. ESRI User Conference, San Diego, CA. https://env761.github.io/assets/files/tpi-poster-tnc_18x22.pdf.

Xu, H., 2006. Modification of normalised difference water index (NDWI) to enhance open water features in remotely sensed imagery. Int. J. Remote Sens. 27 (14), 3025–3033. https://doi.org/10.1080/01431160600589179.

Xu, J., Morris, P.J., Liu, J., Holden, J., 2018. PEATMAP: refining estimates of global peatland distribution based on a meta-analysis. CATENA 160, 134–140. https://doi.org/10.1016/j.catena.2017.09.010.